The inverse autotransporters of *Yersinia ruckeri*, YrInv and YrIlm, contribute to biofilm formation and virulence

Agnieszka Wrobel,[1] Athanasios Saragliadis,[1]
Jesús Pérez-Ortega [ID],[2] Carolin Sittman,[3]
Stephan Göttig,[3] Krystyna Liskiewicz,[1]
Maria Helle Spence,[1] Kenneth Schneider [ID],[1]
Jack C. Leo [ID],[1,4] Jesús Arenas[2,5†] and Dirk Linke [ID][1*†]

[1]Department of Biosciences, University of Oslo, 0316, Oslo, Norway.

[2]Department of Molecular Microbiology and Institute of Biomembranes, Utrecht University, Utrecht, The Netherlands.

[3]Institute of Medical Microbiology and Infection Control, Hospital of Johann Wolfgang Goethe-University, Frankfurt am Main, Germany.

[4]Department of Biosciences, School of Science and Technology, Nottingham Trent University, Nottingham, NG1 4FQ, UK.

[5]Unit of Microbiology of the Department of Animal Pathology, University of Zaragoza, Zaragoza, Spain.

Summary

Yersinia ruckeri **causes enteric redmouth disease (ERM) that mainly affects salmonid fishes and leads to significant economic losses in the aquaculture industry. An increasing number of outbreaks and the lack of effective vaccines against some serotypes necessitates novel measures to control ERM. Importantly,** *Y. ruckeri* **survives in the environment for long periods, presumably by forming biofilms. How the pathogen forms biofilms and which molecular factors are involved in this process, remains unclear.** *Yersinia ruckeri* **produces two surface-exposed adhesins, belonging to the inverse autotransporters (IATs), called** *Y. ruckeri* **invasin (YrInv) and** *Y. ruckeri* **invasin-like molecule (YrIlm). Here, we investigated whether YrInv and YrIlm play a role in biofilm formation and virulence. Functional assays revealed that YrInv and YrIlm promote biofilm formation on different abiotic substrates. Confocal microscopy revealed that they are involved in microcolony interaction and formation, respectively. The effect of both IATs on biofilm formation correlated with the presence of different biopolymers in the biofilm matrix, including extracellular DNA, RNA and proteins. Moreover, YrInv and YrIlm contributed to virulence in the** *Galleria mellonella* **infection model. Taken together, we propose that both IATs are possible targets for the development of novel diagnostic and preventative strategies to control ERM.**

Introduction

Yersinia ruckeri is a Gram-negative bacterium and the causative agent of enteric redmouth disease (ERM) (Ross *et al*., 1966; Rucker, 1966; Kumar *et al*., 2015; Wrobel *et al*., 2019). *Yersinia ruckeri* strains can be differentiated based on their biotypes (biotype 1 and biotype 2), serotypes (O1a; O2a, b, c; O3 and O4) and outer membrane protein profiles. Strains of serotype O1 are the major cause of ERM, also referred to as yersiniosis. ERM affects wild fish and fish culture, in particular rainbow trout and Atlantic salmon. The clinical characteristics of ERM include haemorrhages found on the fish skin and mucosal surfaces, as well as exophthalmia, also known as 'pop-eye' (Kumar *et al*., 2015). Vaccination and antibiotic treatment are the current strategies used to control the disease; however, the number of outbreaks, particularly in Atlantic salmon, has substantially increased worldwide in recent years (Hjeltnes *et al*., 2017), suggesting that the pathogen is adapting to acquired host immune responses and antimicrobial treatments. Therefore, ERM is considered as an emerging infectious disease, and there is an urgent need for novel control measures.

A key factor is the capacity of the bacteria to survive in the environment under adverse conditions for long periods of time, possibly through the production of resistance structures, such as biofilms. Biofilms are organized communities of microorganisms that adhere to each other and to surfaces through a self-produced extracellular matrix. This provides a stable microenvironment, in which bacterial cells can resist antibiotics, disinfectants, free radicals and temperature variations (Yin *et al*., 2019). Biofilms in aquatic environments are a source of

recurrent infections leading to large fish losses (Cai *et al*., 2013). *Y. ruckeri* can form biofilms that resist oxolinic acid treatment (Coquet *et al*., 2002). The molecular basis of how *Y. ruckeri* produces biofilms has not been investigated in detail. Biofilm formation in *Y. ruckeri* seems to be regulated through quorum-sensing homoserine lactones (Torabi Delshad *et al*., 2019) and by catecholamines (Torabi Delshad *et al*., 2019).

Type V secretion systems are used by Gram-negative bacteria for secretion of a variety of protein fibres, adhesins and enzymes to the cell surface. This class of secretion systems is divided into five groups (Va–e) that comprise (i) autotransporters (Va, Vc–e) and (ii) two-partner secretion systems (type Vb) (Leo *et al*., 2012). The main difference between both groups resides in the translocation mechanism through the outer membrane. Autotransporters are translocated with the help of the general β-barrel assembly machinery (Bam) complex, whereas proteins secreted by the two-partner secretion system use a specific outer membrane transporter, called TpsB. Bam recognizes and inserts transmembrane β-barrel proteins into the bacterial outer membrane, and all autotransporters contain such a β-barrel domain, also termed the 'translocator domain' (Leo *et al*., 2012; Fan *et al*., 2016). The translocator domain is located at the C-terminal region in most of the autotransporters (Va, Vc and Vd) or at the N-terminus in IATs (Ve). Once the translocator domain is inserted in the membrane, it helps to export the so-called 'passenger' or extracellular effector domain of the autotransporter, probably assisted by the Bam machinery (Leo and Linke, 2018). Passengers can remain anchored at the cell surface or can be released into the medium. Many autotransporters play an important role in bacterial pathogenesis, including processes such as cleavage of host proteins, adhesion, microcolony formation, biofilm formation and auto-aggregation (Meuskens *et al*., 2019). In particular, IATs share a common domain architecture, and some were shown to promote bacterial adhesion to host cells (Leo *et al*., 2015). Typical examples of IATs are intimin from enterohemorrhagic *Escherichia coli* (Jerse *et al*., 1990) and InvA from enteropathogenic *Yersiniae* (Isberg *et al*., 1987).

We recently identified two genes coding for two IATs in *Y. ruckeri*, namely *yrInv* (for *Y. ruckeri* invasin) and *yrIlm* (for *Y. ruckeri* invasin-like molecule) (Leo *et al*., 2015; Wrobel *et al*., 2017). Their corresponding proteins are composed of an N-terminal signal peptide, a short periplasmic region containing a peptidoglycan-binding LysM minidomain, a translocator domain as well as a large, repetitive passenger domain made of immunoglobulin (Ig)-like domains, capped by a C-type lectin domain at the C-terminus in each case. YrIlm is composed of a

variable number of Ig-like domains depending on the strain, usually 20, whereas YrInv always contains three Ig-like domains. The expression of YrInv and YrIlm is regulated by environmental factors such as temperature, osmolarity, iron availability as well as the presence of nutrients (Wrobel *et al*., 2017). Many IATs are involved in biofilm formation, such as FdeC, IatC and YeeJ from *E. coli*, and EtInvA from *Edwardsiella tarda* (Nesta *et al*., 2012; Dong *et al*., 2013; Martinez-Gil *et al*., 2017; Goh *et al*., 2019). We therefore hypothesized that YrInv and YrIlm may play a role in biofilm formation and virulence of *Y. ruckeri*. To verify this hypothesis, we used the model strain *Y. ruckeri* NVH_3758 and a variety of functional *in vitro* and *in vivo* assays.

Results

YrInv is localized on the bacterial cell surface

Bacterial attachment to surfaces is the first step in biofilm formation. The attachment can be mediated by a number of different surface-exposed bacterial structures such as lipoproteins (Kovacs-Simon *et al*., 2011), autotransporters (Linke *et al*., 2006; Benz and Schmidt, 2011; Meuskens *et al*., 2019) and two partner secretion proteins (Guérin *et al*., 2017), pili and fimbriae (Lukaszczyk *et al*., 2019) that protrude from the cell surface and mediate the initial attachment to the substrate (Klemm and Schembri, 2000). To determine whether YrInv is surface-exposed, we used a Spytag-SpyCatcher system developed by Zakeri *et al*. (Zakeri *et al*., 2012) and further modified by us (Chauhan *et al*., 2019). The Spytag is a short peptide that forms a covalent isopeptide bond with its binding partner, the protein SpyCatcher. In our experiments, we did not include YrIlm, due to its repetitive nature (19 repeat units of 300 bp each, located in the passenger) and the resulting difficulty in cloning. We produced two variants of SpyCatcher, both containing superfolder green fluorescent protein (sfGFP), namely sfGFP-fused SpyCatcher and sfGFP-fused SpyCatcherEQ. The latter is a non-reactive variant of SpyCatcher due to a point mutation in its active site and thus serves as a negative control. A recombinant YrInv with a Spytag at the C-terminus was engineered and expressed in *E. coli* BL21-Gold (DE3). The resulting strain was called Ec_YrInv[+]. Ec_YrInv^{+} cells were incubated separately with sfGFP-fused SpyCatcher and sfGFP-fused SpyCatcherEQ as negative control. Intact cells of Ec_YrInv[+] became fluorescent after excitation, whereas our negative control remained non-fluorescent (Fig. 1A). Quantification of the fluorescence intensity showed that adding sfGFP-fused SpyCatcher to of Ec_YrInv[+] resulted in 4- and 4.5-fold higher fluorescence emission compared to adding sfGFP-fused SpyCatcherEQ or to

uninduced cells, respectively. As sfGFP-SpyCatcher is unable to cross the outer membrane, these results indicate that the passenger domain of YrInv was translocated through the outer membrane and remains exposed at the cell surface.

YrInv and YrIIm play a role in biofilm formation

We next determined whether both IATs facilitate biofilm formation. To address this question, the biofilm formation of *Y. ruckeri* NVH_3758, and corresponding single and double knockout strains were studied under static growth conditions at 22°C on polystyrene plates. After different growth periods, the biofilm biomass was quantified by crystal violet staining. Strain NVH_3758 produced quantifiable and stable biofilms after 48 h of growth; however, we did not detect significant and reproducible biofilms at earlier time points using this technique. Biofilm formation of the mutant strains NVH_3758Δ*yrInv* and NVH_3758Δ*yrIIm* produced less biofilm biomass than the parent strain (Fig. 2), 70% and 60%, respectively. Nevertheless, this reduction was not statistically significant because of variation between biological replicates. However, the original biofilm biomass production could be restored to levels even higher than the wildtype (NVH_3758) when YrInv and YrIIm were expressed *in trans* (Fig. 2). This suggests that both IATs contribute to biofilm production. To understand the contribution of both IATs, we tested the biofilm produced by the double knockout mutant next. We detected a statistically significant reduction of biomass production, down to 30% as compared to the NVH_3758 strain (Fig. 2), suggesting that the effect of the two IATs on biofilm formation is independent and additive. To rule out that the biofilm formation phenotypes were not based on growth defects, the growth characteristics of the NVH_3758 strain and the corresponding single mutant derivatives were evaluated under shaking conditions. NVH_3758 and mutants showed similar growth characteristics during the lag and logarithmic phase; however, the mutants showed a delay at the beginning of the stationary phase, which was even more pronounced in the double mutant (Supplementary Fig. 1A). Biofilms were typically detected towards the end of the 48 h growth experiments in all strains. When we measured the number of cells in the culture medium at the end of the biofilm formation experiment, the amount of planktonic cells was higher for the double mutant compared to the NVH_3758 (Supplementary Fig. 1B). We hypothesize that the reduction in biofilm biomass is mainly due to reduced adhesion of cells to the substrate rather than reduced growth. Together, these results indicate that both IATs facilitate biofilm formation of *Y. ruckeri*.
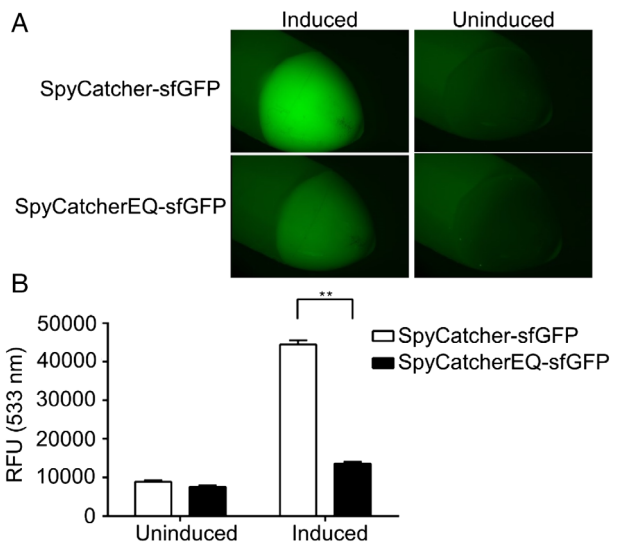

Fig. 1. Localization of a full-length YrInv at the *E. coli* BL21-Gold (DE3) surface. A. Spytag-SpyCatcher binding assay with the full-length YrInv localized at the *E. coli* BL21-Gold (DE3) surface. sfGFP-fused SpyCatcher or sfGFP-fused SpyCatcherEQ (a non-reactive SpyCatcher variant used as a negative control) were added to *E. coli*BL21-Gold (DE3) cells expressing Spytag-YrInv. Both mixtures were then incubated for 30 min, washed, centrifuged, and the pellets were imaged using a fluorescent microscope with a magnification 7,82× (Leica M205 FA) directly in the 1.5 ml centrifuge tubes. The two images on the left show induced *E. coli* BL21-Gold (DE3) cell pellets expressing Spytag-YrInv bound to sfGFP-fused SpyCatcher (top) and sfGFP-fused SpyCatcherEQ (bottom), respectively. The two images on the right show uninduced *E. coli* BL21-Gold (DE3) cell pellets bound to sfGFP-fused SpyCatcher (top) and sfGFP-fused SpyCatcherEQ (bottom), respectively. B. Relative fluorescence of induced and uninduced *E. coli* BL21-Gold (DE3) cells bound to sfGFP-fused SpyCatcher and SpyCatcherEQ, measured with a plate reader. Bacterial cultures were added to a 96-well plate and fluorescence at 533 nm (sfGFP) was measured with an excitation peak at the wavelength 488 nm. The level of fluorescence is given in relative fluorescence units (RFU). The data presents means and standard deviations of three independent experiments. Statistically significant differences between samples are indicated with asterisks (**$p < 0.01$). The p value was calculated by one-way ANOVA followed by a Dunnett's multiple comparison test. The error bars indicate standard deviations. [Color figure can be viewed at wileyonlinelibrary.com]

Yersinia ruckeri produces biofilms on different substrate materials

We evaluated the influence of both IATs on the capacity of *Y. ruckeri* to form biofilms on materials commonly used in aquaculture: wood, polyvinyl chloride (PVC), polystyrene, ceramic (water filter medium) and steel. These materials are components of fish cages (wood), fish tanks (steel, PVC), aquaculture buoys (polystyrene), pipes (PVC) and oxygen diffusers and filter material (ceramic). The surfaces were characterized by optical profilometry, so that we could relate biofilm production with the nature of the material and its surface morphology. The following morphological parameters were determined: arithmetic mean height (Sa, mean surface roughness), root mean square height (Sq), skewness

(Ssk, asymmetry of the height distribution) and kurtosis (Sku, flatness of the height distribution). The resulting values for each material are listed in Table 1, and examples of the surface morphology are depicted in Fig. 3A. Overall, the materials showed diverse surface morphologies. The surface roughness was lowest for the polished stainless steel samples and highest for the filter ceramics. Despite this, stainless steel showed the sharpest surface features (Sku), whereas polystyrene presente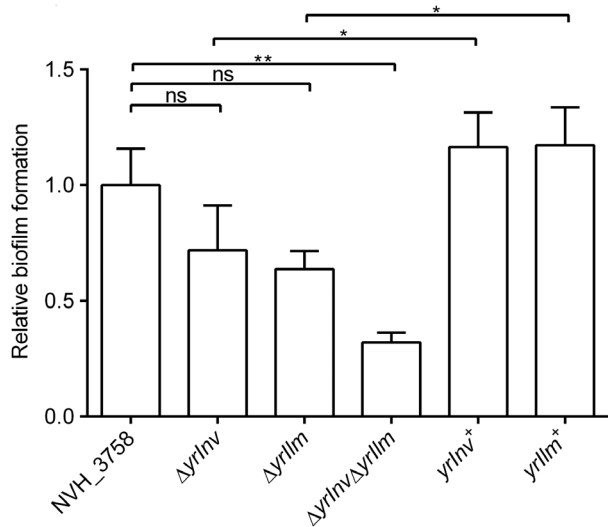d the most rounded. The most negative value for surface skewness (Ssk) was measured for stainless steel, and the largest positive value was obtained from wood.

Thereafter, we quantified the colonization capacity of *Y. ruckeri* on the characterized materials. To this end, bacterial cultures were deposited on the material surface. After 48 h of growth, biofilms were disrupted by incubation with Proteinase K and bacterial loads were quantified by CFU enumeration. We chose this method because it did not alter cell viability; however, it is important to note that a small number of bacteria may still be retained on the substrate. Statistical comparisons revealed significant differences in the number of bacteria recovered from the materials (Fig. 3B), likely reflecting different adhesive capacities. Steel, ceramic and PVC released the lowest and highest number of bacteria, respectively (Fig. 3B). Thus, biofilm formation of *Y. ruckeri* is strongly dependent on the nature of the substrate. We next evaluated the contribution of IATs on biofilm formation on these materials (Fig. 3C). IAT mutants were poorly recovered from all the materials as compared with wildtype with one exception (double mutant Δ*yrlnv*Δ*yrllm* from wood). The fact that steel and ceramic represented the surfaces with the lowest and the highest mean surface roughness, respectively, indicates that neither Sa nor Sq were decisive parameters for *Yersinia* adhesion. However, both surfaces can be considered hydrophilic, in contrast to the other materials, suggesting that *Y. ruckeri* adheres better to hydrophobic surfaces. *Y. ruckeri* cells are generally hydrophilic, but become slightly more hydrophobic in stationary growth phase (Coquet *et al*., 2002), and thus potentially also in biofilm growth.

Deletion of IATs influenced the amount of *Yersinia* recovered from PVC to the greatest extent compared to the other tested materials. NVH_3758 Δ*yrlnv* or NVH_3758 Δ*yrllm* mutants were hardly recovered (less than half of the NVH_3758's CFU density), and we did not recover the double knockout mutant (Fig. 3C). This indicates that the production of both IATs is crucial for the adhesion of *Yersinia* to PVC. The PVC surface

Fig. 2. Biofilm formation of *Y. ruckeri* NVH_3758 and its IAT knockout strains under static growth conditions. Biofilm formation by the *Y. ruckeri* NVH_3758 strain and the deletion mutants a measured by crystal violet staining. The data show the mean of three biological replicates, expressed relative to the *Y. ruckeri* NVH_3758 strain. Error bars indicate standard deviations between these biological replicates. Statistically significant differences between samples are indicated with asterisks (*$p < 0.05$, **$p < 0.01$, ns = not significant). The *p* values were calculated by one-way ANOVA followed by a Dunnett's multiple comparison test. The error bars indicate standard deviations.

Table 1. Surface characterization of various biofilm substrates (stainless steel, polyvinyl chloride, polystyrene, wood, ceramic) determined by optical profilometry at magnification of 150× (samples ≥ 8). The surface height parameters are as follows: arithmetic mean height (mean surface roughness) Sa, root mean square height Sq, skewness (asymmetry of the height distribution) Ssk and kurtosis (flatness of the height distribution) Sku.

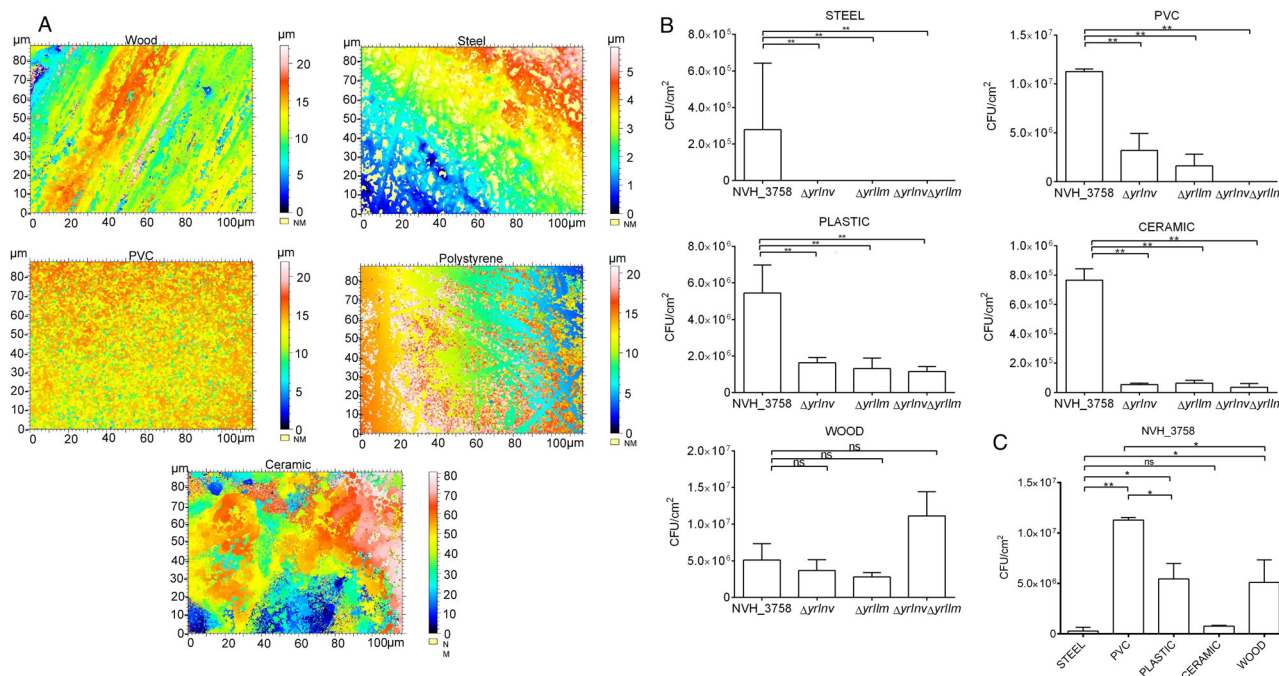|	Materials									
	Stainless steel		Polyvinyl chloride		Polystyrene		Wood		Ceramic	
	Mean	SD	Mean	SD	Mean	SD	Mean	SD	Mean	SD
Sa (μm)	0.211	0.041	1.183	0.051	3.149	0.267	2.757	1.431	11.208	1.611
Sq (μm)	0.294	0.071	1.496	0.058	3.584	0.219	3.786	2.025	13.678	1.831
Ssk	−1.167	0.603	−0.893	0.102	0.290	0.303	0.555	0.641	−0.349	0.209
Sku	7.405	2.756	4.329	0.353	1.910	0.197	5.288	2.329	2.637	0.292

SD, standard deviation.

Fig. 3. Biofilm formation of *Y. ruckeri* NVH_3758 and its mutant strains on materials found in aquaculture. A. The topography layers of all tested materials (wood, steel, PVC, polystyrene, ceramic) using optical profilometry. B. Substrate alters the biofilm formation capacity of *Y. ruckeri* NVH_3758. Of note, 2 x 10⁹ CFU of *Y. ruckeri* NVH_3758 were added into a 12-well plate containing material discs and incubated for biofilm formation. The disc-attached bacteria were recovered through physical and enzymatic treatments and determined by CFU counting and expressed in CFU cm⁻². The data show the average of three biological replicates. Error bars indicate standard deviations between the three biological replicates. C. Impact of IATs on the biofilm formation of strain NVH_3758 on different materials. Experiments and analysis were performed as described in panel B. For B and C, statistically significant differences between samples were marked with asterisks (*$p < 0.05$, **$p < 0.01$, ns = not significant). [Color figure can be viewed at wileyonlinelibrary.com]

ranked as the second lowest for Sa and Sq, possessed a negative skewness and showed a kurtosis value of approximately 4.3 (Table 1). A value of 3 representing a perfect Gaussian distribution and >3 meaning that surface features are narrower than a Gaussian distribution (Saurí *et al.*, 2015). The PVC surface shapes were therefore not so different from the stainless steel surface (Fig. 3A), from which we recovered a reduced number of bacteria (Fig. 3B). The main difference in surface shape to PVC was the steel kurtosis value of 7.4, meaning that the steel surface exhibited sharper surface features (Fig. 3A). Polystyrene showed a similar declining trend in biofilm formation upon deletion of IATs, and only differed from PVC in having a slightly positive skewness and much rounder surface features (Sku = 1.9). The opposite trend was observed for the wood surface, where single IAT knockouts did not significantly change the *Y. ruckeri* capacity to form biofilms, and the double knockout actually increased the CFU density to similar values as observed for the wildtype on PVC. This indicates a potential repulsion between IATs and wood, which does not completely prevent *Y. ruckeri* NVH_3758 binding, and is only eliminated, if both IATs are deleted. Together, these

results suggest a role of IATs as key adhesins for *Y. ruckeri* adherence to different surfaces.

YrInv and YrIlm contribute differently to Y. ruckeri *biofilm structure*

To investigate the biofilm of *Y. ruckeri* in more detail, fluorescent strains were generated in wildtype and IATs derivative mutants, and the biofilm structure was examined by confocal laser scanning microscopy. Figure 4A shows the biofilm architecture of *Y. ruckeri* NVH_3758 and derivative mutants after 48 h of growth. NVH_3758 biofilms constituted large, elongated cell clusters (large bacterial aggregates) that were connected to each other and surrounded by small microcolonies (small cell aggregates) and single cells. Biofilms formed by the NVH_3758ΔyrInv mutant also contained large aggregates that, in contrast to the parent, hardly interacted, thus generating segregated clusters. Biofilms generated by the NVH_3758ΔyrIlm mutant consisted of microcolonies and single cells that were randomly dispersed over the substrate and hardly formed clusters. Biofilms formed by the double mutant showed isolated small microcolonies and single cells.
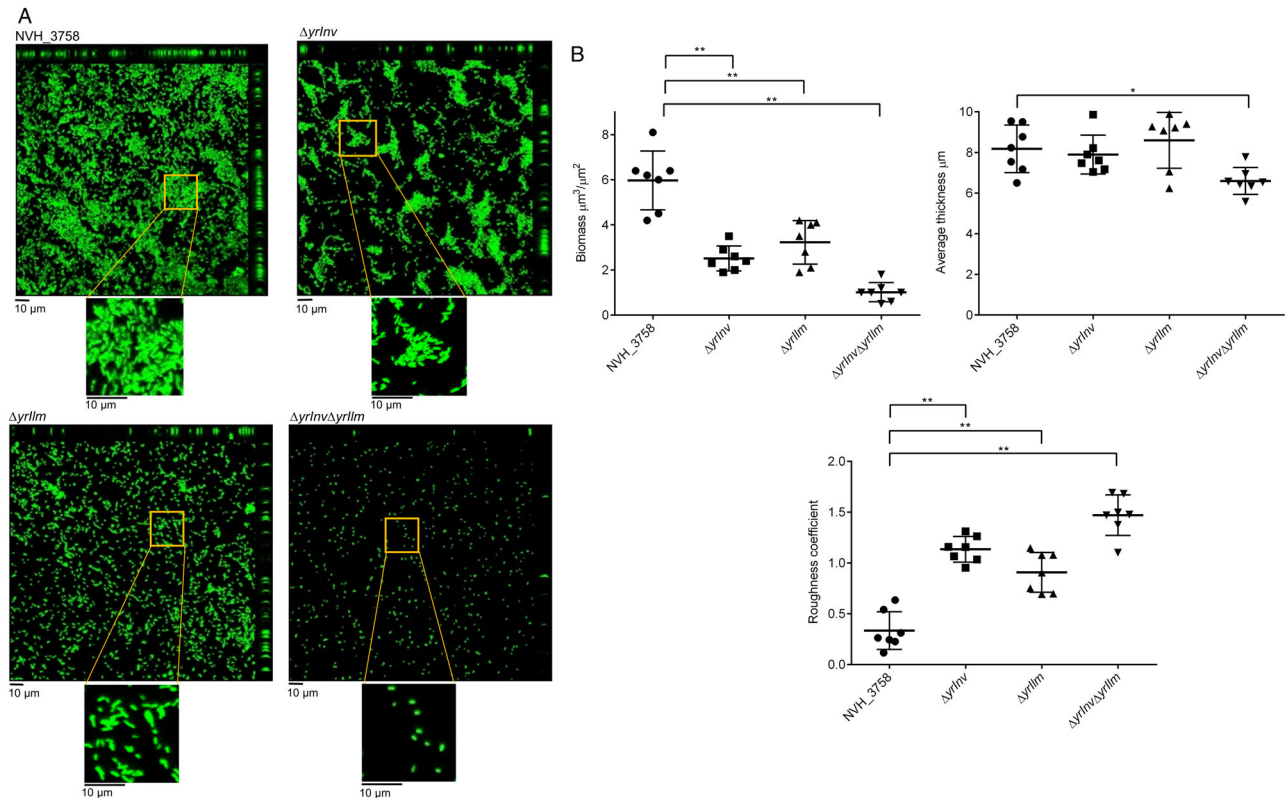
Fig. 4. Biofilm architecture of *Y. ruckeri* NVH_3758 and IATs mutant derivatives. A. Spatial organization of 48 h biofilms formed by NVH_3758 and IAT knockout strains and visualized by confocal laser scanning microscopy. In the enlargements, the interbacterial interactions on the biofilm are highlighted. In the wildtype, bacterial clusters interact with each other; in the Δ*yrlnv* mutant, bacterial clusters have a reduced interaction each other; in the Δ*yrllm* mutant, bacteria form microcolonies but fail to form clusters; in the Δ*yrlnv*Δ*yrllm* mutant, bacteria can hardly form micro-colonies. The images are representative for at least three independent experiments. B. Biomass, average thickness, and roughness coefficient of biofilms of *Y. ruckeri* NVH_3758 and IAT knockout strains were analysed by COMSTAT (Heydorn *et al*., 2000). The presented values were deter-mined based on the average of seven image stacks from a representative experiment. Statistically significant differences between samples are indicated with asterisks (*$p < 0.05$, **$p < 0.01$). The p values were calculated by one-way ANOVA followed by a Dunnett's multiple comparison test. The error bars indicate standard deviations. [Color figure can be viewed at wileyonlinelibrary.com]

This analysis confirmed our preliminary observations that YrInv and YrIlm might have additive, but not identi-cal functions; YrIlm induces microcolony formation, whereas YrInv has a role in connecting these microcolonies. Clearly, these data point out that both IATs have a relevant role in diverse interbacterial interactions. However, as we did not quantify auto-aggregation in liquid cultures, the observed pheno-types could be derived from bacteria-bacteria and/or bacteria-substrate interactions. We applied COMSTAT analysis to further characterize the contribution of these effects to the biofilm structure (Fig. 4B). Results revealed a higher biofilm biomass in the NVH_3758 than was achieved with single and double mutant derivatives, in agreement with our crystal violet staining assays (Fig. 2). COMSTAT analysis also showed a deviating biofilm thickness in the double mutant and a higher roughness coefficient in the mutants as compared to the NVH_3758. Overall, these

data support the conclusion that the natural structure of *Y. ruckeri* biofilms depends on the expression of both IATs.

Extracellular DNA (eDNA), RNA and proteins are components of Y. ruckeri *biofilms*

The biofilm matrix is highly variable among species and can be composed of proteins, exopolysaccharides, eDNA, cell membranes and RNA. We investigated the role of some of these biofilm matrix components and the role of IATs by exogenous addition of DNase I, RNase A or Proteinase K to growing cultures and studied their effect on biofilm biomass through crystal violet staining. Addition of DNase I, RNase A or Proteinase K to NVH_3758 reduced the biofilm biomass production sig-nificantly, down to about 40% compared to untreated bio-films (Fig. 5A). Addition of these enzymes did not effect
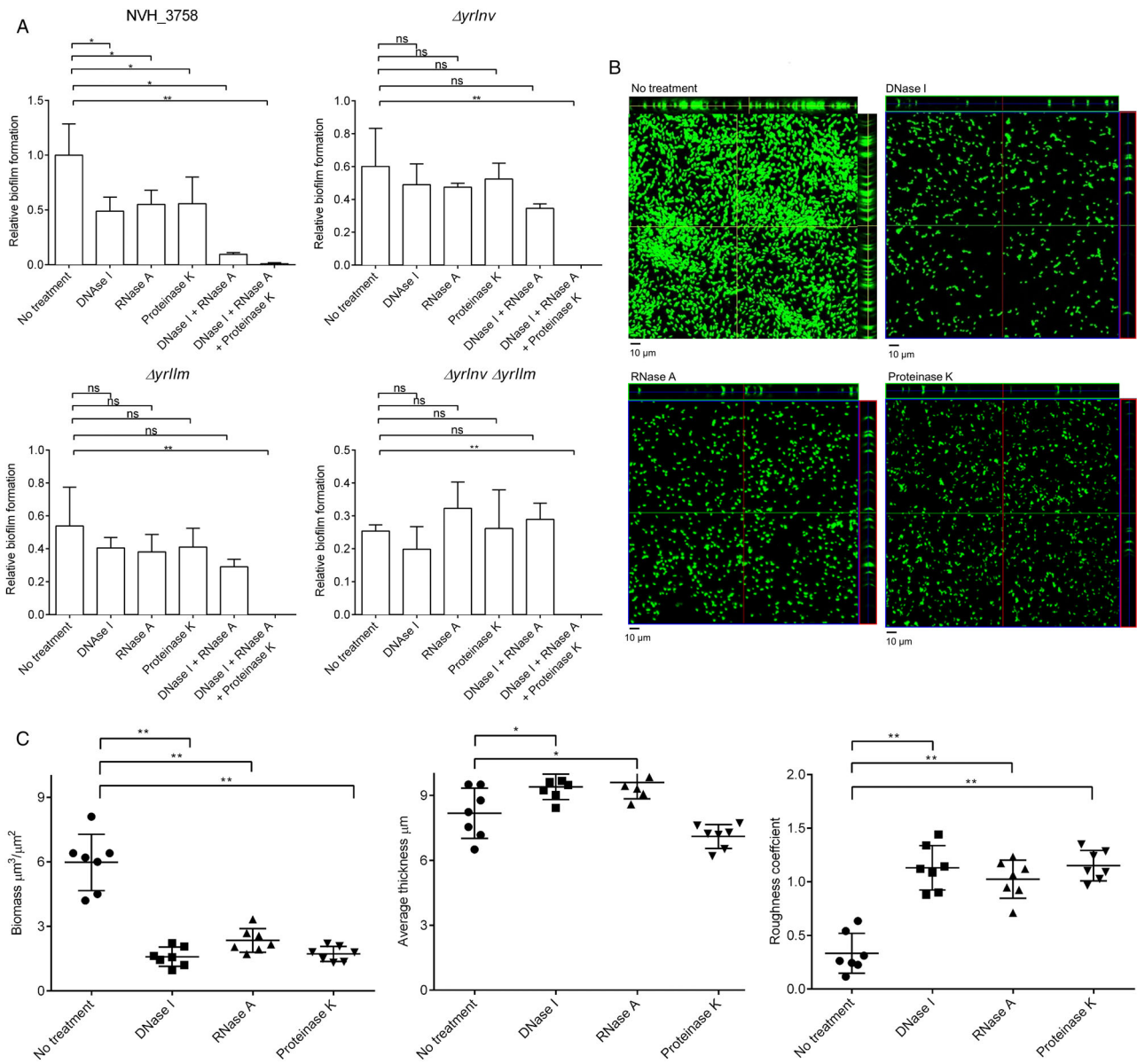
Fig. 5. Biofilm formation of the *Y. ruckeri* strains treated with different enzyme combinations. A. Biofilm formation of the *Y. ruckeri* NVH_3758 strain and the deletion mutants of *yrInv* and *yrIlm* treated with DNase I, RNase A and Proteinase K. Biofilms were formed in a 24-well plate at 28°C, and where indicated, enzymes were added to the *Y. ruckeri* cultures, incubated for 48 h and biofilm biomass quantified using crystal violet. The data show the mean of three biological replicates, expressed relative to the *Y. ruckeri* NVH_3758 strain. Error bars indicate standard deviations between the three biological replicates. Statistically significant differences between samples are indicated with asterisks (*$p < 0.05$, **$p < 0.01$, ns = not significant). The p values were calculated by one-way ANOVA followed by a Dunnett's multiple comparison test. The error bars indicate standard deviations. B. Confocal microscopy images of biofilm structures developed by the *Y. ruckeri* NVH_3758 strain treated with a single enzyme (either DNase I, RNase A or Proteinase K) under static conditions. The images were obtained using confocal laser scanning microscopy and are representative for at least three independent experiments. C. Biomass, average thickness and roughness coefficient of biofilm of the *Y. ruckeri* NVH_3758 strain treated with a single enzyme (DNase I, RNase A or Proteinase K) analysed by COMSTAT (Heydorn *et al*., 2000). The presented values were determined based on the average of seven image stacks from a representative experiment. Statistically significant differences between samples are indicated with asterisks (*$p < 0.05$, **$p < 0.01$). The p values were calculated by one-way ANOVA followed by a Dunnett's multiple comparison test. The error bars indicate standard deviations. [Color figure can be viewed at wileyonlinelibrary.com]

bacterial viability (data not shown). Simultaneous addition of DNase I and RNase A reduced the biofilm biomass even further, to 10% of the untreated control, and addition of the three enzymes together abolished biofilm formation completely (Fig. 5A). Combined addition of the three enzymes abolished biofilm formation for all mutants as well; however, in contrast to the NVH_3758, addition of only one or two enzymes had a minimal impact

(Fig. 5A). Microscopic inspection of the NVH_3758 biofilms revealed that microcolony formation was largely inhibited by the three treatments (Fig. 5B). Note in the orthogonal views, the differences in the volume of the clusters and the variable number and length of interspersed spaces within the biomass of enzyme-treated biofilms. COMSTAT analysis of these biofilms revealed that separate addition of the three enzymes reduced the biofilm biomass and increased the roughness coefficient as compared to the untreated control (Fig. 5C). Together, these results demonstrate that the *Y. ruckeri* biofilm matrix requires the presence of DNA, RNA and proteins for proper biofilm formation. To visualize the presence of eDNA on biofilms, we stained biofilms with propidium iodide, which binds to DNA and produces red fluorescence. The propidium iodide is not able to cross the cellular membrane of live cells and thus, only eDNA can be stained. To facilitate colocalization studies, we analysed 24 h old biofilms of strain NVH_3758 and its double mutant derivative Δ*yrInv*Δ*yrIlm*. Bacterial clusters of strain NVH_3758 were abundantly stained with propidium

iodide (Fig. 6A). These bacterial clusters were constituted by green cells (without eDNA), red cells (dead cells) and yellow cells (live cells with attached eDNA) (see enlargement of merged figure in the right panel). Colocalization of stained DNA within cells, expressed as Pearson's R values, revealed a good correlation of 0.8. Biofilms of the double mutant Δ*yrInv*Δ*yrIlm* contained a reduced number of yellow and red cells. Pearson's R analysis revealed a significantly lower correlation for the double mutant (0.6, Fig. 6B). Overall, these assays confirmed the existence of eDNA on biofilms of NVH_3758, which seems to be related to microcolony formation and the production of IATs.

YrInv and YrIlm contribute to virulence in vivo

Finally, we evaluated the contribution of YrInv and YrIlm to *Y. ruckeri* virulence using the *Galleria mellonella* (larvae of the greater wax moth) infection model, which has extensively been used to analyse pathogenicity of Gram-negative bacteria (Tsai *et al*., 2016; Tietgen *et al*., 2018).
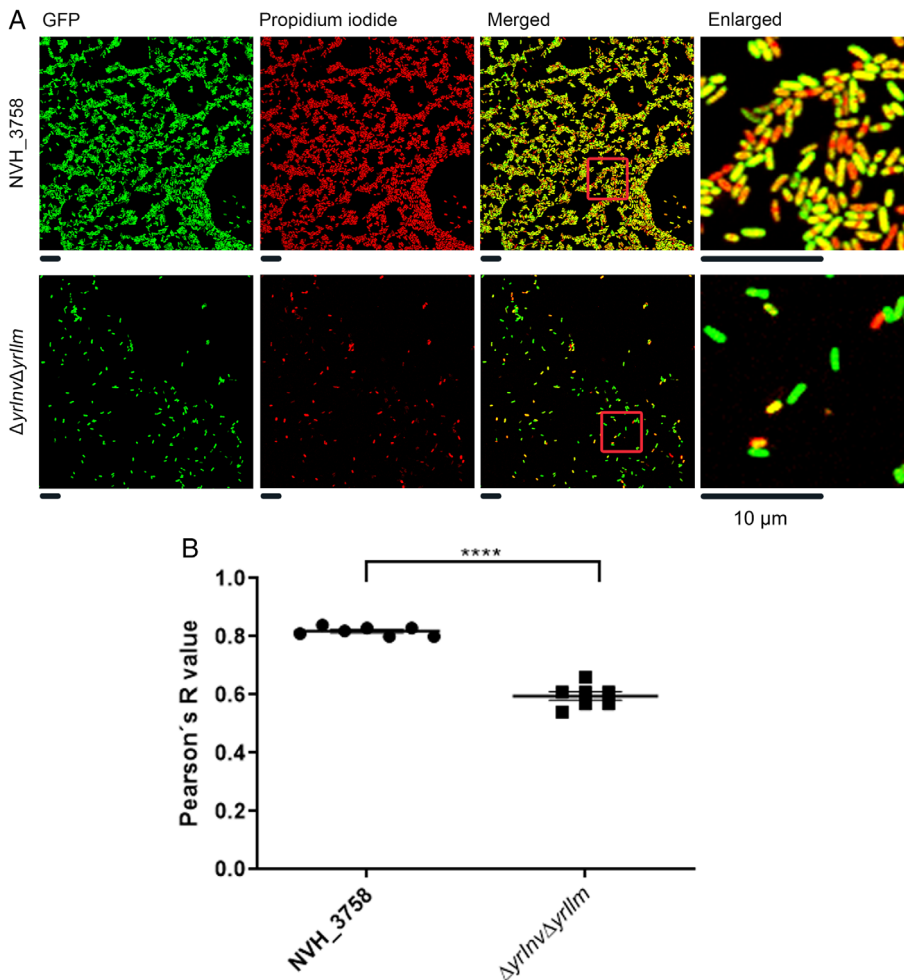

Fig. 6. Visualization of DNA on *Y. ruckeri* biofilms. A. Distribution of propidium iodide-stained DNA (red-fluorescence) within 24 h old biofilms of *Y. ruckeri* NVH_3758 and its Δ*yrInv*Δ*yrIlm* mutant derivative. Both bacterial strains produce a superfolded GFP protein (green-fluorescence). Representative images acquired with individual and combined fluorescence are displayed. B. Quantification of the colocalization of eDNA within cells expressed as Pearson's R values. Colocalization was quantified using the Coloc 2 plugin in the image processing environment ImageJ. Pearson's *R* values of 1 indicate perfect correlation and of 0 no correlation. Data were calculated from eight random images of biofilms from a representative experiment of three and expressed as mean and standard error of the mean. Statistically significant differences between samples were calculated with an unpaired *t* test and indicated with asterisks (****$p < 0.0001$). [Color figure can be viewed at wileyonlinelibrary.com]

G. mellonella larvae were injected with serially diluted bacterial suspensions of the NVH_3758 strain, and the median lethal dose that killed 50% (LD_{50}) of the larvae was calculated by monitoring the larvae survival over time (Supplementary Fig. S2).

The wild-type strain had a $\log_{10} LD_{50}$ of 4.95 after 24 h and of 4.74 after 48 h (Table 2). The mean $\log_{10} LD_{50}$ values for single and double IAT mutant strains were significantly higher than the parent strain, ranging between 5.26 and 5.39 after 24 h and 5.07 and 5.21 after 48 h, indicating a diminished killing of *G. mellonella* larvae compared to the wild-type (Table 2). These results suggest that YrInv and YrIlm contribute directly to bacterial virulence *in vivo*.

Discussion

The aim of this study was to elucidate the contribution of two IATs, YrInv and YrIlm of *Y. ruckeri*, to biofilm formation and virulence. In the enteropathogenic *Yersiniae*, Invasin, the orthologue of YrInv, plays a key role in virulence (Chauhan *et al*., 2016). Invasin is expressed in the first phase of infection in both *Y. enterocolitica* and *Y. pseudotuberculosis*, and mediates binding to β_1 integrins, which eventually leads to tissue invasion of the bacteria. It is thus possible that either YrInv or YrIlm may play a similar role in colonization of fish tissues. IAT involvement in virulence towards fish has been shown for EtInvA of *E. tarda* (Dong *et al*., 2013).

We employed the *G. mellonella in vivo* infection model to analyse virulence of *Y. ruckeri* and the impact of *yrInv* and *yrIlm*. The transcription of both IATs is upregulated at higher temperatures (Wrobel *et al*., 2017), which matches with their presumed role as virulence factors. Hence, we grew *Yersinia* at 37°C (Champion *et al*., 2009). All *Y. ruckeri* strains showed a time and dosedependent killing of larvae with a $\log_{10} LD_{50}$ of approximately 10^5, which is comparable to other important pathogens like *Escherichia coli*, *Klebsiella*

Table 2. Logarithmic median lethal doses (log LD_{50}) of *Y. ruckeri* strains in larvae of *G. mellonella* at 24 h and 48 h after infection. Each value was calculated from four independent infection experiments each employing four different bacterial CFU and 10 larvae/ CFU.

Y. ruckeri strain	24 h		48 h	
	log LD_{50}	95% CI	log LD_{50}	95% CI
NVH_3758	4.95	[4.81–5.08]	4.74	[4.57–4.91]
NVH_3758Δ*yrIlm*	5.28	[5.21–5.34]	5.07	[4.93–5.21]
NVH_3758Δ*yrInv*	5.39	[5.20–5.58]	5.21	[5.05–5.36]
NVH_3758 Δ*yrIlm*Δ*yrInv*	5.26	[5.14–5.37]	5.12	[4.98–5.26]

CI, confidence interval.

pneumoniae or *Acinetobacter baumannii* (Tietgen *et al*., 2018; Weidensdorfer *et al*., 2019) thereby underlining the pathogenicity of *Y. ruckeri*. Deletion of *yrInv* or *yrIlm* or both reduced virulence by 50% compared to NVH_3758, which indicates that both IATs contribute modestly to virulence without showing a synergy in this infection model. Our results demonstrate a direct, but not very strong effect in the knockout mutants. Thus, further research on possible receptors for these adhesins on fish cells should be performed in the future.

In this study, we established biofilm assays for *Y. ruckeri* that yielded reproducible biofilms and were used to characterize determinants of biofilm formation and biofilm architecture. Nothing was known about *Y. ruckeri* biofilm architecture when we started this work, and we started by using different enzymes on the biofilm matrix, showing that it comprises both protein and nucleic acid components. We showed that the architecture of *Y. ruckeri* biofilms is constituted by dispersed, but interconnected, microcolonies. A similar structure was recently described for *Y. enterocolitica* (Lenchenko *et al*., 2019). Many IATs from other organisms, particularly *E. coli* and the fish pathogen *E. tarda*, have been implicated in biofilm formation (Nesta *et al*., 2012; Dong *et al*., 2013; Martinez-Gil *et al*., 2017; Goh *et al*., 2019). Therefore, we also investigated the role of the two *Y. ruckeri* IATs in our biofilm model. Our results indicated that YrInv and YrIlm mediate inter-bacterial interactions during biofilm biogenesis and that this activity directly influences biofilm architecture and biomass. Single and double knockout strains revealed that although *Yersinia* YrIlm induces microcolony formation, YrInv has a role in connecting these microcolonies. Considering that the double knockout mutant strain produced only 30% of the biomass of NVH_3758, these results may suggest that interbacterial interactions are crucial for *Y. ruckeri* biofilm formation. However, it is also possible that IATs may have a dual role in substrate binding and inter-bacterial interactions. In any case, results of Fig. 5 suggest that these interactions could be facilitated through the interaction of both IATs with components of the extracellular matrix. Bacterial biofilms are composed of cells producing extracellular matrix polymers including RNA, DNA, proteins, lipids and polysaccharides. eDNA, especially, has been suggested to play an essential role in bacterial attachment (Harmsen *et al*., 2010). By using combinations of hydrolytic enzymes, we showed that RNA, DNA and protein components are involved in forming the biofilm matrix of *Y. ruckeri*. Microscopy assays evidenced that eDNA is fully associated to microcolonies, suggesting its importance in microcolony formation (Fig. 6). Both YrInv and YrIlm contain a passenger domain consisting of Ig-like domains capped by a C-type lectin-like domain that could be responsible for substrate binding. Lectins are often

highly specific binders of carbohydrates (Elgavish and Shaanan, 1997). It is tempting to speculate that the *Y. ruckeri* IATs might bind eDNA, RNA or other matrix components facilitating the interaction with each other or with the substrate (Fig. 6A), as largely demonstrated for other autotransporters and surface exposed proteins of different pathogens (Arenas and Tommassen, 2017). Further molecular binding studies will elucidate the role of these two surface-exposed proteins in the process of biofilm formation in more detail.

Many fish pathogens are able to colonize surfaces and form biofilms in aquaculture facilities. These biofilms act as reservoirs of the pathogen that can lead to recurrent outbreaks. Previous studies have shown that fish pathogens can be easily recovered from surfaces commonly found in aquaculture (Cai *et al*., 2013). Coquet *et al*. (2002) showed that *Y. ruckeri* is able to form a biofilm on wooden, concrete, PVC and fibreglass supports found in rainbow trout farms (Coquet *et al*., 2002). We found that also under controlled laboratory conditions *Y. ruckeri* produces biofilms on different abiotic materials, including those commonly used in aquaculture. The adhesion and proliferation of bacteria on material surfaces has been shown to be affected by material composition, surface charge and surface morphology (Renner and Weibel, 2011). Surface morphology comprises various parameters, such as roughness, skewness and kurtosis. Both Sa and Sq describe the general height variation of the surface; however, these parameters do not describe the shape of the surface structures. The additional parameters Ssk and Sku were therefore chosen and are described in detail by Hansson *et al*. and Crawford *et al*. (Hansson and Hansson, 2011; Crawford *et al*., 2012). Briefly, Ssk indicates if a surface is more dominated by peaks with wide valleys (positive value), or by narrow crevices with wide plateaus between them (negative value). Sku is a measure of the sharpness of the surface features. For *Y. ruckeri*, we found indications that surface roughness, more than skewness and kurtosis, influences biofilm formation, confirming that surface roughness and the presence of flagella played a major role in biofilm formation (Coquet *et al*., 2002; Coquet *et al*., 2002). This suggests that biofilms in aquaculture systems could be managed by improving the surface morphology of the materials used. But in our hands, hydrophobicity and surface charge of the abiotic surface seem to have a stronger influence on IAT binding than the surface morphology, at least in a static assay. The value of static assays is that these interactions can be investigated without too much interference from surface morphology, thereby simplifying the system of determining factors for adhesion. Both PVC and polystyrene are hydrophobic surfaces, which distinguishes them from hydrophilic steel, ceramic (sintered glass) and wood surfaces (van

Loosdrecht *et al*., 1990; Zhang *et al*., 2018). Adhesion to hydrophilic surfaces is dominated by electrostatic forces, whereas adhesion to hydrophobic surfaces depends more on Van der Waals interactions (Oliveira *et al*., 2001). It is therefore most likely that IAT binding is mediated by non-polar parts of the proteins.

In contrast to our findings, an earlier study by Coquet *et al*. found a strong correlation between material surface roughness and *Y. ruckeri* adhesion (Coquet *et al*., 2002). Their study investigated the adhesion of two WT strains to similar fish culture materials (wood, concrete, PVC and fibreglass); however, biofilms were grown under gyratory agitation with 115 r.p.m. Coquet *et al*. provided an excellent example for the increasing influence of surface morphology on adhesion, if shear flow is introduced. This highlights the importance of investigating adhesion in a static assay before approximating the real-life situation in a more complex environment, especially if adhesin function is studied. The binding interactions between adhesin and surface (or adhesin and receptor) can easily be masked by shear flow, resulting in the false impression that average surface roughness is the sole determinant for adhesion. In fish culture, the extent of biofilm formation is, of course, also governed by shear flow from moving liquid. Future work should thus include biofilm formation assays under shear flow, where the influence of surface roughness on adhesion can be expected to increase. In addition, it should be noted that we tested the micro-scale roughness and not the nano-scale roughness, to maintain a consistent measurement area for all surface parameters. The nano-scale roughness trend among these materials might differ from micro-scale roughness.

Interestingly, both single knockout strains used in this study exhibited the same colonization pattern on different materials, with the strongest adhesion to wood. The double knockout strain, however, exhibited an even stronger adhesion to wood compared to single knockout strains. This increase in adhesion to wood upon the deletion of both IATS strongly suggests that additional factors contribute to adhesion and biofilm formation, and that these are unmasked only in the double knockout strain. This is in analogy to the *Y. enterocolitica* adhesin Ail that acts only in the absence of other adhesins (Biedzka-Sarek *et al*., 2008; Tsang *et al*., 2013).

Many autotransporters in diverse Gram-negative pathogens, for example YapC, EibD, NalP, AutA and UpaG, have been implicated in biofilm formation (Valle *et al*., 2008; Leo *et al*., 2011; Arenas *et al*., 2013, 2014; Chauhan *et al*., 2016). Recently, a widespread IAT family of *E. coli*, exemplified by YeeJ and FdeC, was shown to contribute to biofilm formation. YeeJ is a very large protein (2358 amino acids). Overexpression of YeeJ in *E. coli* MG1655 significantly increased the biofilm

formation compared to the WT *E. coli* MG1655 strain (Nesta *et al*., 2012; Martinez-Gil *et al*., 2017). Bioinformatics analysis showed that YeeJ, like other IATs, contains a LysM domain, which binds to peptidoglycan and stabilizes the proteins as shown previously for another *E. coli* IAT, Intimin (Leo *et al*., 2015). The deletion of the LysM domain of YeeJ resulted in a reduction of surface exposure of YeeJ and affected biofilm formation (Martinez-Gil *et al*., 2017). FdeC is involved in the adhesion of *E. coli* cells to mammalian cells and extracellular matrix components. *Escherichia coli* strains constitutively expressing FdeC were shown to interact with solid surfaces by forming bacterial aggregates (Nesta *et al*., 2012). Even more recently, three other biofilm-promoting IATs, IatBCD, have been described from an environmental isolate of *E. coli* (Goh *et al*., 2019). Notably, Dong *et al*. (2013) who investigated the role of the Invasin orthologue EtInvA in the fish pathogen of *Edwardsiella tarda* found that EtInvA contributes to biofilm formation (Dong *et al*., 2013). Our work is in agreement with these previous findings on the role of autotransporters as virulence factors, suggesting that they can be used as relevant diagnostic markers and vaccine candidates.

Experimental procedures

Bacterial strains, growth conditions and colony-forming units determination

The strains and plasmids used in this study are listed in Table 3. *Yersinia ruckeri* NVH_3758 strain was kindly provided by the Norwegian Veterinary Institute in Oslo, Norway, and was originally isolated from an ERM outbreak in farmed Atlantic salmon in Norway in 1987 (Wasteson *et al*., 1989). *Escherichia coli* CC118λ*pir+* and *E. coli* β2163Δ*nic* were kindly supplied by Dr. Monika Schütz from the Institute for Medical Microbiology and Hygiene, University Hospital in Tübingen, Germany. All strains were grown in lysogeny broth (Bertani, 1951) (LB) at 28°C or 37°C for *Y. ruckeri* and *E. coli*, respectively. When required, appropriate antibiotics were added to the medium at the following final concentrations: 10 μg ml^{-1} tetracycline, 50 μg ml^{-1} kanamycin and 100 μg ml^{-1} ampicillin.

Overnight liquid cultures of *Y. ruckeri* were adjusted to an optical density of 0.01 at 600 nm (OD$_{600}$) to determine the growth curve. Then, 5 μl of the adjusted bacterial culture were added to 200 μl sterile culture medium and placed in a 96-well plate. The plates were sealed with a BreathEasy membrane from Sigma-Aldrich. The OD$_{600}$ was measured every 20 min until the bacteria reached the stationary phase, using a Synergy H1 plate reader (Biotek). The experiment was repeated three times.

To determine the number of colony-forming units (CFU), bacteria were diluted 1:100 from an overnight culture into fresh LB medium with 0.5% NaCl and grown to 1.0 OD$_{600}$. Samples were then serially diluted, mixed with top agar and plated on LB plates. Three technical replicates were performed for each CFU count. Similar CFU counts were performed to test the effect of enzymes used in this study (RNAse, DNAse, Proteinase K – see below) on bacterial vitality. In this case, serial dilutions were made after incubating cultures at 1.0 OD$_{600}$ for 2 h with an enzyme concentration of 0.1 mg ml^{-1}.

Generation of Y. ruckeri *mutants*

To prepare deletion mutants in *yrInv* and *yrIlm*, two DNA fragments downstream (608 bp for *yrInv* and 530 bp for *yrIlm*) and upstream (1134 bp for *yrInv* and 562 bp for *yrIlm*) of the selected genes were amplified by PCR from *Y. ruckeri* NVH_3758 genomic DNA using primers pairs described in Supplementary Table 1. For primer design, public genomes were used: GenBank accession no. CP023184, *yrInv*: 262571–265099; *yrIlm*: 3493041–3500852). The two DNA fragments were fused employing Splicing by Overlap Extension PCR (Herrero *et al*., 1990). The resulting DNA fragment was cloned into suicide plasmid pSB890Y using Gibson Assembly (Gibson *et al*., 2009). Successful cloning was verified by PCR and further sequencing, and the plasmid was propagated in *E. coli* strains harbouring the *pir* gene. Following this, the construct was re-transformed into *E. coli* β2168Δ*nic35*, a conjugative strain and *m*-diaminopimelic acid auxotroph, and later introduced into *Y. ruckeri* NVH_3758 via conjugation (Weirich *et al*., 2017). The resulting transconjugants were screened on LB agar supplemented with 10 μg ml^{-1} tetracycline to select *Y. ruckeri* tetracycline resistant merodiploids. Subsequently, the *Y. ruckeri* merodiploids were counterselected on LB agar with 10% of sucrose to select clones that had lost the *sacB*-containing plasmid. *sacB* encodes the enzyme levansucrase that converts sucrose into a toxic product (Weirich *et al*., 2017). Only the strains that have lost the suicide plasmid through a second recombination event will grow on sucrose-containing plates. The resulting deletion mutants were confirmed by PCR using primers flanking the deleted locus and genomic DNA as the template and then sequencing the PCR product (Table 3). The confirmed mutant strains were called NVH_3758Δ*yrInv* and NVH_3758Δ*yrIlm*. Likewise, a double mutant strain was generated and called NVH_3758Δ*yrInv*Δ*yrIlm*.

To produce complemented strains, called NVH_3758*yrInv*$^+$ and NVH_3758*yrIlm*$^+$, a DNA fragment containing the native promoter and the intact full-length DNA sequence of the selected genes was amplified from genomic DNA of *Y. ruckeri* NVH_3758. Subsequently, the DNA fragment was cloned into pUC19 using Gibson

Table 3. Strains and plasmids used in this study.

Strains/plasmids	Characteristics	References
Y. ruckeri NVH_3758	*Y. ruckeri* strain isolated from farmed Atlantic salmon in Norway	(Gulla *et al*., 2018)
NVH_3758Δ*yrInv*	NVH_3758 where *yrInv* was deleted leaving a clean deletion mutant	This study
NVH_3758Δ*yrIlm*	NVH_3758 where *yrIlm* was deleted leaving a clean deletion mutant	This study
NVH_3758Δ*yrInv*Δ*yrIlm*	NVH_3758 where *yrIlm* and *yrInv* were deleted leaving a clean deletion mutant	This study
NVH_3758*yrInv*$^+$	NVH_3758 *yrInv* complementation strain, Amp^R	This study
NVH_3758*yrIlm*$^+$	NVH_3758 *yrIlm* complementation strain, Amp^R	This study
E. coli CC118λ*pir*$^+$	Δ(*ara-leu*) *araD*Δ*lacX74 galE galK phoA20 thi-1 rpsE rpoB argE*(Am) *recA1λpir* phage lysogen	(Herrero *et al*., 1990)
E. coli β2163Δ*nic*	F⁻*RP4-2-Tc::Mu*Δ*dapA::*(*erm-pir*), Km^{R}Em^{R}Δ*nic*	(Demarre *et al*., 2005)
E. coli BL21-Gold (DE3)	*E. coli* B F⁻*dcm* $^+$ Hte *ompT hsdS* (r$_B$- m$_B$-) *gal λ* (DE3) *endA* Tet^R	(Studier and Moffatt, 1986)
E. coli TOP10	F⁻*mcrA*Δ(*mrr-hsdRMS-mcrBC*) Φ80*lacZ*ΔM15Δ*lacX74 nupG recA1araD139*Δ(*ara-leu*)7697 *galE15 galK16rpsL*(Str^R) *endA1 λ*	Invitrogen
pSB890Y	Suicide plasmid, Tet^R, *sacB*	(Hapfelmeier *et al*., 2004; Weirich *et al*., 2017)
pUC19	Cloning vector, Amp^R	
pUC19_*yrInv*	Complementation plasmid containing a full-length *yrInv* with a native signal peptide, Amp^R	This study
pUC19_*yrIlm*	Complementation plasmid containing a full-length *yrIlm* with a native signal peptide, Amp^R	This study
pKK289:sfGFP	Complementation plasmid containing a full-length *sfgfp*, Km^R	(Bönquist *et al*., 2008)
pASK_IBA3_*yrInv*_SpyTag	For producing full-length YrInv with C-terminal SpyTag, Amp^R	This study

assembly. The resulting constructs were confirmed by sequencing and electroporated (see below) into *Y. ruckeri* strain NVH_3758Δ*yrInv* and strain NVH_3758Δ*yrIlm*, respectively.

To prepare fluorescent mutants for microscopy purposes, a pKK289:sfGFP plasmid encoding superfolder green fluorescent protein (Lampe *et al*., 2017) was used. The pKK289:sfGFP plasmid was introduced into *Y. ruckeri* cells by electroporation. Briefly, *Y. ruckeri* culture was grown up to an OD$_{600}$ of 0.2, washed twice with ice-cold water and resuspended in ice-cold 10% glycerol. Subsequently, 50 ng of DNA was added to ice-cold *Y. ruckeri* cells, and the mixture was incubated for another 20 min on ice. After incubation, the mixture was pulsed in 0.2 cm gap electroporation cuvettes at 2.5 kV, 200 ω and 25 μF. The cells were immediately recovered in SOC medium for 45 min at 28°C (Hanahan, 1983) and plated on LB agar medium supplemented with 50 μg ml^{-1} of kanamycin.

Localization of *Y. ruckeri YrInv*

Localization of *Y. ruckeri* YrInv was performed by applying the SpyTag-SpyCatcher system. SpyCatcher is a protein that recognizes a specific 11-residue peptide (SpyTag); upon recognition, a covalent isopeptide bond is formed (Zakeri *et al*., 2012). The system can be used for mapping the localization or topology of OM proteins, as the SpyCatcher protein cannot penetrate the OM. Therefore, only SpyTags exposed on the extracellular surface of the cell can react with SpyCatcher. For easy readout, SpyCatcher can be fused to fluorescent proteins such as sfGFP (Chauhan *et al*., 2019; Hatlem *et al*., 2019). *Escherichia coli* BL21-Gold (DE3) was transformed with the plasmid pASK_IBA3_*yrInv*_SpyTag, which contains an intact *yrInv* gene and its own promoter, followed by a DNA sequence encoding for a SpyTag before the stop codon. The transformants were cultured in LB medium at 30°C to an OD$_{600}$ of 0.5, and expression of *yrInv* was induced by adding anhydrotetracycline to a final concentration of 0.05 μg ml^{-1}. After induction, cells were grown until the OD$_{600}$ reached 1.0, after which they were harvested and resuspended in 1.5 ml PBS. Then, 5 μM of either purified sfGFP-fused SpyCatcher or 5 μM of purified sfGFP-fused SpyCatcherEQ (used as a negative control, as this variant is non-reactive and does not form the covalent bond with SpyTag) was added to the collected cells (both induced and uninduced) (Chauhan *et al*., 2019). The resulting mixtures were incubated for 30 min at room temperature. After this, the cells were washed three times with phosphate-buffered saline (PBS), and fluorescent images of cells were taken with an epifluorescent microscope (Leica M205 FA, Leica Microsystems). Finally, relative fluorescence of cells bound

to sfGFP-fused SpyCatcher was quantified with a Biotek Synergy1 plate reader. For this purpose, 100 μl of cell suspension was added to a 96-well plate, and fluorescence of sfGFP was measured with excitation at 488 nm and emission at 507 nm.

Biofilm formation in microtiter plates

Quantification of biofilm formation was performed in microtiter plates as described earlier (Arenas *et al*., 2013) with minor modifications. First, overnight cultures of *Y. ruckeri* strains were adjusted to an OD_{600} of 1, corresponding to 2×10^9 CFU. Subsequently, 500 μl of bacterial cultures were inoculated into 24-well plates. Where indicated, DNase I, RNase A and Proteinase K were added to the *Y. ruckeri* culture to a final concentration of 100 μg ml^{-1}. At these concentrations, CFU counts were not affected by the presence of the enzymes after 2 h incubation (data not shown). The bacteria were then incubated statically at 28°C for different time intervals. When required, the biofilm was treated with all three enzymes; DNase I and RNase A were added first for 48 h, followed by the addition of Proteinase K for further 2 h to avoid the degradation of the nucleases by Proteinase K. After incubation, the bacterial cultures were removed from the plate and the adherent bacteria were washed once with PBS. For biofilm quantification, bacterial biofilm was stained with 0.5% crystal violet for 2 min, washed three times with PBS and air-dried for 5–10 min. Finally, the biofilm was solubilized with 33% acetic acid and quantified relative to an abiotic control using a spectrophotometer at a wavelength of 630 nm.

Biofilm formation on different materials

Biofilm formation by the *Y. ruckeri* strains was investigated on different materials: PVC, wood (untreated oak that had been sanded), polystyrene (obtained from a Nunc 24-Well Plate, ThermoFisher), ceramics/sintered glass (aquarium filter medium, EHEIM Substrat, EHEIM GmbH, Germany) and polished stainless steel (AISI 316L). All materials had a disc shape of 8 mm diameter (with the exception of ceramic, which had a disc diameter of 6 mm), were 1 mm thick and were sterilized before the experiments by autoclaving. First, overnight cultures of *Y. ruckeri* strains were adjusted to an OD_{600} of 1 and 500 μl of the adjusted culture were added into a 12-well plate. Three discs prepared from the same material were placed in each well. The plate was then incubated for 48 h at 28°C. After incubation, the discs were washed once with PBS and removed from the plate. All three discs were swabbed with a single swab. The swabs were then placed in 500 μl of sterile water containing 100 μg ml^{-1} of Proteinase K for microcolony disruption. Next,

serial dilutions of the resulting mixture were prepared and spread on LB-solid medium and incubated at 28°C for 24 h. After incubation, the bacteria were counted and the results were expressed as CFU/ml per cm^2 of material. The experiment was repeated three times.

Imaging and biofilm analysis

Biofilm structures were visualized and analysed by confocal microscopy. Forty-eight hours-old biofilms grown on glass coverslips were chemically fixed with PBS containing 2% formaldehyde for 2 h as previously described (Pérez-Ortega *et al*., 2017). For visualization of eDNA within biofilms, 24 h old biofilms were fixed and incubated with a solution containing 1 μl ml^{-1} propidium iodide (P3566, Invitrogen) in physiological salt for 15 min at room temperature in dark. Images were taken using Zeiss LSM 700 confocal laser scanning microscopes (Carl Zeiss, Germany), equipped with a 40×/1.30 Plan-Neofluar oil and 63×/1.40 Plan-Apochromat oil objective immersion objectives respectively. Multiple images were taken with 0.4 μm Z-intervals. The biomass, average thickness and roughness coefficient were analysed using the computer program COMSTAT (Heydorn *et al*., 2000). For colocalization of eDNA within bacterial cells on biofilm, the Coloc 2 plugin in the image processing environment ImageJ was used (v1.48, NIH, http://imagej.nih.gov/ij/). Each experiment was performed at least in duplicate.

Surface morphology characterization by profilometry

The material surfaces for biofilm formation were characterized by green light (530 nm) optical profilometry (S neox; Sensofar) at 150× magnification (Nikon-EPI confocal objectives), with a scanning area of 116 × 87 μm. All surface characterization was performed in the absence of biological material. Using clean material discs, three-dimensional images were acquired through focus variation and were analysed with the software SensoMAP (Sensofar) for the following height parameters: arithmetic mean height (Sa, mean surface roughness), root mean square height of the surface (Sq), skewness (Ssk, asymmetry of the height distribution) and kurtosis (Sku, flatness of the height distribution), described by (Sauri *et al*., 2015). All presented values are the arithmetic mean of measurements in at least eight randomly chosen locations.

Galleria mellonella *infection experiments*

Larvae of the greater wax moth (*G. mellonella*) were obtained from UK Waxworm (Sheffield, UK) or Bio-Systems Technology (Exeter, UK) and used as an *in vivo* model to assess virulence of *Y. ruckeri* strains. Sentinels

(approximately one per 50 larvae) were homogenized and plated on Columbia blood agar to screen for bacterial colonization. After 24 h incubation, species identification of the respective colonies was done by matrix-assisted laser desorption/ionization mass spectrometry (Vitek® MS, bioMérieux). Batches with contamination of Gram-negative bacteria were discarded (Tietgen *et al.*, 2018). The *Y. ruckeri* strains were cultivated in brain heart infusion by inoculation of fresh medium with an overnight culture. Bacteria were cultivated at $37°C$ and 180 r.p.m. shaking until an OD_{600} of 0.4 was reached. Bacteria were adjusted to an OD_{600} of 1 in PBS and serially diluted. For generation of time-kill curves, 10–12 larvae of the respective strain were infected with 10 μl of serial diluted bacterial suspensions (range: 1×10^3 to 1×10^7 CFU) by injection into the hemocoel via the last left proleg using Hamilton precision syringes. PBS was used as a negative control. Infected caterpillars were incubated in Petri dishes at $37°C$ for up to 96 h, and survival was monitored. Larvae were considered dead if they repeatedly did not respond to touch. The median lethal dose (LD_{50}) was calculated by nonlinear regression analysis using GraphPad Prism 5 (GraphPad, La Jolla) as (Marra *et al.*, 2012; Tietgen *et al.*, 2018).

Statistical analysis

Data from at least three independent experiments were used for statistical analysis. Regarding biofilm formation experiments, data were presented relative to the NVH_3758 values, which were set to 1. Biofilm structure was characterized based on seven image stacks of each sample, which were generated from representative experiments. Statistical analyses were performed with one-way ANOVA, followed by a Dunnett's multiple comparison test using the GraphPad Prism 6.0 software. Data derived from colocalization studies were compared with an unpaired *t* test using GraphPad Prism 6.0 software. The *p* values were considered significant when $*p \leq 0.5$, $**p \leq 0.01$ and $****p < 0.0001$. Analyses of LD_{50} values were performed using the Extra sum-of-squares *F* test using GraphPad Prism.

Acknowledgements

Sources of funding

Disclosures

The authors declare that the research was conducted in the absence of any commercial or financial relationships that could be construed as a potential conflict of interest.

Ethics statement

Infection experiments with *Galleria mellonella* do not require ethical approval.

Author contributions

AW and DL conceived the study; AW, DL and JA designed the experiments; AW, KL, MS, JP, AS, CS, SG and KS carried out the experiments; AW, JA, JCL and DL contributed to the discussion and interpretation of the data; AW wrote the first draft of the manuscript with contributions from JA, KS and SG. All authors provided critical feedback and contributed to the final shape of the manuscript.

References

Arenas, J., Cano, S., Nijland, R., van Dongen, V., Rutten, L., van der Ende, A., and Tommassen, J. (2014) The meningococcal autotransporter AutA is implicated in autoaggregation and biofilm formation. *Environ Microbiol* **17**: 1321–1337.

Arenas, J., Nijland, R., Rodriguez, F.J., Bosma, T.N.P., and Tommassen, J. (2013) Involvement of three meningococcal surface-exposed proteins, the heparin-binding protein NhbA, the α-peptide of IgA protease and the autotransporter protease NalP, in initiation of biofilm formation. *Mol Microbiol* **87**: 254–268.

Arenas, J., and Tommassen, J. (2017) Meningococcal biofilm formation: Let's stick together. *Trends Microbiol* **25**: 113–124.

Benz, I., and Schmidt, M. (2011) Structures and functions of autotransporter proteins in microbial pathogens. *Int J Med Microbiol* **301**: 461–468.

Bertani, G. (1951) Studies on lysogenesis. The mode of phage liberation by lysogenic *Escherichia coli*. *J Bacteriol* **62**: 293–300.

Biedzka-Sarek, M., Salmenlinna, S., Gruber, M., Lupas, A., Meri, S., and Skurnik, M. (2008) Functional mapping of

YadA- and ail-mediated binding of human factor H to *Yersinia enterocolitica* serotype O:3. *Infect Immun* **76**: 5016–5027.

Bönquist, L., Lindgren, H., Golovliov, I., Guina, T., and Sjöstedt, A. (2008) MglA and Igl proteins contribute to the modulation of *Francisella tularensis* live vaccine strain-containing phagosomes in murine macrophages. *Infect Immun* **76**: 3502–3510.

Cai, W., De La Fuente, L., and Arias, C.R. (2013) Biofilm formation by the fish pathogen *Flavobacterium Columnare*: development and parameters affecting surface attachment. *Appl Environ Microbiol* **79**: 5633–5642.

Champion, O., Cooper, I., James, S., Ford, D., Karlyshev, A., Wren, B., *et al*. (2009) *Galleria mellonella* as an alternative infection model for *Yersinia pseudotuberculosis*. *Microbiology* **155**: 1516–1522.

Chauhan, N., Hatlem, D., Orwick-Rydmark, M., Schneide, K., Floetenmeyer, M., Rossum, B., *et al*. (2019) Insights into the autotransport process of a trimeric autotransporter, *Yersinia* adhesin A (YadA). *Mol Biol* **111**: 844–862.

Chauhan, N., Wrobel, A., Skurnik, M., and Leo, J. (2016) *Yersinia* adhesins: an arsenal for infection. *Proteomics - Clin Appl* **10**: 949–963.

Coquet, L., Cosette, P., Junter, G.-A., Beucher, E., Saiter, J.-M., and Jouenne, T. (2002) Adhesion of *Yersinia ruckeri* to fish farm materials: influence of cell and material surface properties. *Colloids Surf B* **26**: 373–378.

Coquet, L., Cosette, P., Quillet, L., Petit, F., Junter, G., and Jouenne, T. (2002) Occurrence and phenotypic characterization of *Yersinia ruckeri* strains with biofilm-forming capacity in a rainbow trout farm. *Appl Environ Microbiol* **68**: 470–475.

Crawford, R., Webb, H., Truong, V., Hasan, J., and Ivanova, E. (2012) Surface topographical factors influencing bacterial attachment. *Adv Colloid Interface Sci* **179–182**: 142–149.

Demarre, G., Guérout, A., Matsumoto-Mashimo, C., Rowe-Magnus, D., Marlière, P., and Mazel, D. (2005) A new family of mobilizable suicide plasmids based on broad host range R388 plasmid (IncW) and RP4 plasmid (IncPα) conjugative machineries and their cognate *Escherichia coli* host strains. *Res Microbiol* **156**: 245–255.

Dong, X., Fan, X., Wang, B., Shi, X., and Zhang, X.-H. (2013) Invasin of *Edwardsiella tarda* is essential for its haemolytic activity, biofilm formation and virulence towards fish. *J Appl Microbiol* **115**: 12–19.

Elgavish, S., and Shaanan, B. (1997) Lectin-carbohydrate interactions: different folds, common recognition principles. *Trends Biochem Sci* **22**: 462–467.

Fan, E., Chauhan, N., Udatha, D., Leo, J., and Linke, D. (2016) Type V secretion systems in bacteria. *Microbiol Spectr* **4**: 1–24.

Gibson, D., Young, L., Chuang, R., Venter, J., Hutchiso, C., and Smith, H. (2009) Enzymatic assembly of DNA molecules up to several hundred kilobases. *Nat Methods* **6**: 343–345.

Goh, K., Moriel, D., Hancock, S., Phan, M., and Schembri, M. (2019) Bioinformatic and molecular analysis of inverse autotransporters from *Escherichia coli*. *mSphere* **4**: 1–12.

Guérin, J., Bigot, S., Schneider, R., Buchanan, S.K., and Jacob-Dubuisson, F. (2017) Two-partner secretion: combining efficiency and simplicity in the secretion of large proteins for bacteria-host and bacteria-bacteria interactions. *Front Cell Infect Microbiol* **7**: 1–23.

Gulla, S., Barnes, A., Welch, T., Romalde, J., Ryder, D., Ormsby, M., *et al*. (2018) Multi-locus variable number of tandem repeat analysis (MLVA) of *Yersinia ruckeri* confirms the existence of host-specificity, geographic endemism and anthropogenic dissemination of virulent clones. *Appl Environ Microbiol* **84**: 1–6.

Hanahan, D. (1983) Studies on transformation of *Escherichia coli* with plasmids. *J Mol Biol* **166**: 557–580.

Hansson, K., and Hansson, S. (2011) Skewness and kurtosis: important parameters in the characterization of dental implant surface roughness—a computer simulation. *ISRN Mater Sci* **2011**: 1–6.

Hapfelmeier, S., Ehrbar, K., Stecher, B., Barthel, M., Kremer, M., and Hardt, W. (2004) Role of the *Salmonella* pathogenicity island 1 effector proteins SipA, SopB, SopE, and SopE2 in *Salmonella enterica* subspecies 1 Serovar typhimurium colitis in streptomycin-pretreated mice. *Infect Immun* **72**: 795–809.

Harmsen, M., Lappann, M., Knøchel, S., and Molin, S. (2010) Role of extracellular DNA during biofilm formation by *Listeria monocytogenes*. *Appl Environ Microbiol* **76**: 2271–2279.

Hatlem, D., Trunk, T., Linke, D., and Leo, J. (2019) Catching a SPY: using the SpyCatcher-SpyTag and related systems for labeling and localizing bacterial proteins. *Int J Mol Sci* **20**: 1–19.

Herrero, M., De Lorenzo, V., and Timmis, K. (1990) Transposon vectors containing non-antibiotic resistance selection markers for cloning and stable chromosomal insertion of foreign genes in Gram-negative bacteria. *J Bacteriol* **172**: 6557–6567.

Heydorn, A., Nielsen, A.T., Hentzer, M., Sternberg, C., Givskov, M., Ersbøll, B.K., and Molin, S. (2000) Quantication of biofilm structures by the novel computer program COMASTAT. *Microbiology* **146**: 2395–2407.

Hjeltnes, B., Bornø, G., Jansen, M., Haukaas, A., and Walde, C. (2017) *The Health Situation in Norwegian Aquaculture 2016*. Oslo, Norway: Norwegian Veterinary Institute Veterinærinstituttet. https://www.vetinst.no/rapporter-og-publikasjoner/rapporter/2017/fish-health-report-2016/.

Isberg, R., Voorhis, D., and Falkow, S. (1987) Identification of invasin: a protein that allows enteric bacteria to penetrate cultured mammalian cells. *Cell* **50**: 769–778.

Jerse, A., Yu, J., Tall, B., and Kaper, J. (1990) A genetic locus of enteropathogenic *Escherichia coli* necessary for the production of attaching and effacing lesions on tissue culture cells. *Proc Natl Acad Sci USA* **87**: 7839–7843.

Klemm, P., and Schembri, M. (2000) Bacterial adhesins: function and structure. *Int J Med Microbiol* **290**: 27–35.

Kovacs-Simon, A., Titball, R., and Michell, S. (2011) Lipoproteins of bacterial pathogens. *Infect Immun* **79**: 548–561.

Kumar, G., Menanteau-Ledouble, S., Saleh, M., and El-Matbouli, M. (2015) *Yersinia ruckeri*, the causative agent of enteric redmouth disease in fish. *Vet Res* **46**: 1–10.

Lampe, E.O., Zingmark, C., Tandberg, J., Thrane, I., Brudal, E., Sjöstedt, A., and Winther-Larsen, H.C. (2017) *Francisella noatunensis* subspecies *noatunensis clpB* deletion mutant impairs development of francisellosis in a zebrafish model. *Vaccine* **35**: 7264–7272.

Lenchenko, E., Lozovoy, D., Strizhakov, A., Vatnikov, Y., Byakhova, V., Kulikov, E., *et al*. (2019) Features of formation of *Yersinia enterocolitica* biofilms. *Vet World* **12**: 136–140.

Leo, J., Grin, I., and Linke, D. (2012) Type V secretion: mechanism(s) of autotransport through the bacterial outer membrane. *Philos Trans R Soc Lond B Biol Sci* **367**: 1088–1101.

Leo, J., and Linke, D. (2018) A unified model for BAM function that takes into account type Vc secretion and species differences in BAM composition. *AIMS Microbiol* **4**: 455–468.

Leo, J., Lyskowski, A., Hattula, K., Hartmann, M., Schwarz, H., Butcher, S., *et al*. (2011) The structure of *E. coli* IgG-binding protein D suggests a general model for bending and binding in trimeric autotransporter adhesins. *Structure* **19**: 1021–1030.

Leo, J., Oberhettinger, P., Chaubey, M., Schütz, M., Kühner, D., Bertsche, U., *et al*. (2015) The Intimin periplasmic domain mediates dimerisation and binding to peptidoglycan. *Mol Microbiol* **95**: 80–100.

Leo, J., Oberhettinger, P., Schütz, M., and Linke, D. (2015) The inverse autotransporter family: Intimin, invasin and related proteins. *Int J Med Microbiol* **305**: 276–282.

Linke, D., Riess, T., Autenrieth, I., Lupas, A., and Kempf, V. (2006) Trimeric autotransporter adhesins: variable structure, common function. *Trends Microbiol* **14**: 264–270.

van Loosdrecht, M., Norde, W., Lyklema, J., and Zehnder, A. (1990) Hydrophobic and electrostatic parameters in bacterial adhesion. *Aquat Sci* **52**: 103–114.

Lukaszczyk, M., Pradhan, B., and Remaut, H. (2019) The biosynthesis and structures of bacterial pili. In *Bacterial Cell Walls and Membranes, Subcellular Biochemistry*, Vol. 92, Kuhn, A. (ed), pp. 369–413). New York: Springer.

Marra, A., Lamb, L., Medina, I., George, D., Gibson, G., Hardink, J., *et al*. (2012) Effect of linezolid on the 50% lethal dose and 50% protective dose in treatment of infections by gram-negative pathogens in naive and immunosuppressed mice and on the efficacy of ciprofloxacin in an acute murine model of septicemia. *Antimicrob Agents Chemother* **56**: 4671–4675.

Martinez-Gil, M., Goh, K.G., Rackaityte, E., Sakamoto, C., Audrain, B., Moriel, D.G., *et al*. (2017) YeeJ is an inverse autotransporter from *Escherichia coli* that binds to peptidoglycan and promotes biofilm formation. *Sci Rep* **7**: 1–16.

Meuskens, I., Saragliadis, A., Leo, J., and Linke, D. (2019) Type V secretion systems: an overview of passenger domain functions. *Front Microbiol* **10**: 1–19.

Nesta, B., Spraggon, G., Alteri, C., Moriel, D., Rosini, R., Veggi, D., *et al*. (2012) FdeC, a novel broadly bonserved *Escherichia coli* adhesin eliciting protection against urinary tract infections. *MBio* **3**: 1–9.

Oliveira, R., Azeredo, J., Teixeira, P., and Fonseca, A. (2001) The role of hydrophobicity in bacterial adhesion. In *Biofilm Community Interact Chance or Necessity Cardiff*,

Gilbert, P., Allison, D., Brading, M., Verran, J., and Walk, J. (eds). UK: Bioline, pp. 11–22.

Pérez-Ortega, J., Rodríguez, A., Ribes, E., Tommassen, J., and Arenas, J. (2017) Interstrain cooperation in meningococcal biofilms: role of autotransporters NalP and AutA. *Front Microbiol* **8**: 1–15.

Renner, L., and Weibel, D. (2011) Physicochemical regulation of biofilm formation. *MRS Bull* **36**: 347–355.

Ross, A., Rucker, R., and Ewing, W. (1966) Description of a bacterium associated with redmouth disease of rainbow trout (*Salmo gairdneri*). *Can J Microbiol* **12**: 763–770.

Rucker, R. (1966) Redmouth disease of rainbow trout (*Salmo gairdneri*). *Bull Off Int Epizoot* **65**: 825–830.

Sauri, J., Sune-Negre, J., Diaz-Marcos, J., Vilana, J., Millan, D., Tico, J.R., *et al*. (2015) Relationships between surface free energy, surface texture parameters and controlled drug release in hydrophilic matrices. *Int J Pharm* **478**: 328–340.

Studier, F., and Moffatt, B. (1986) Use of bacteriophage T7 RNA polymerase to direct selective high-level expression of cloned genes. *J Mol Biol* **189**: 113–130.

Tietgen, M., Semmler, T., Riedel-Christ, S., Kempf, V., Molinaro, A., Ewers, C., and Gottig, S. (2018) Impact of the colistin resistance gene mcr-1 on bacterial fitness. *Int J Antimicrob Agents* **51**: 554–561.

Torabi Delshad, S., Soltanian, S., Sharifiyazdi, H., and Bossier, P. (2019) Effect of catecholamine stress hormones (dopamine and norepinephrine) on growth, swimming motility, biofilm formation and virulence factors of *Yersinia ruckeri in vitro* and an *in vivo* evaluation in rainbow trout. *J Fish Dis Dis* **42**: 477–487.

Tsai, C., Loh, J., and Proft, T. (2016) *Galleria mellonella* infection models for the study of bacterial diseases and for antimicrobial drug testing. *Virulence* **7**: 214–229.

Tsang, T., Wiese, J., Felek, S., Kronshage, M., and Krukonis, E. (2013) Ail proteins of *Yersinia pestis* and *Y. pseudotuberculosis* have different cell binding and invasion activities. *PLoS One* **8**: 1–9.

Valle, J., Mabbett, A., Ulett, G., Toledo-Arana, A., Wecker, K., Totsika, M., *et al*. (2008) UpaG, a new member of the trimeric autotransporter family of adhesins in uropathogenic *Escherichia coli*. *J Bacteriol* **190**: 4147–4161.

Wasteson, U., Hvaal, A., Sorum, H., Myhr, E., and Fossum, K. (1989) Antibacterial spectrum and some other characteristics of an antimicrobial factor produced by *Yersinia ruckeri*. *Acta Vet Scand* **30**: 253–257.

Weidensdorfer, M., Ishikawa, M., Hori, K., Linke, D., Djahanschiri, B., Iruegas, R., *et al*. (2019) The *Acinetobacter* trimeric autotransporter adhesin Ata controls key virulence traits of *Acinetobacter baumannii*. *Virulence* **10**: 68–81.

Weirich, J., Bräutigam, C., Mühlenkamp, M., Franz-Wachtel, M., Macek, B., Meuskens, I., *et al*. (2017) Identifying components required for OMP biogenesis as novel targets for antiinfective drugs. *Virulence* **8**: 1170–1188.

Wrobel, A., Leo, J., and Linke, D. (2019) Overcoming fish defences: the virulence factors of *Yersinia ruckeri*. *Genes (Basel)* **10**: 1–20.

Wrobel, A., Ottoni, C., Leo, J.C., Gulla, S., and Linke, D. (2017) The repeat structure of two paralogous genes,

Yersinia ruckeri Invasin (*yrInv*) and a '*Y. ruckeri* Invasin-like molecule', (*yrIlm*) sheds light on the evolution of adhesive capacities of a fish pathogen. *J Struct Biol* **201**: 171–183.

Yin, W., Wang, Y., Liu, L., and He, J. (2019) Biofilms: the microbial "Protective Clothing" in extreme environments. *Int J Mol Sci* **20**: 1–18.

Zakeri, B., Fierer, J.O., Celik, E., Chittock, E.C., Schwarz-Linek, U., Moy, V.T., and Howarth, M. (2012) Peptide tag forming a rapid covalent bond to a protein, through engineering a bacterial adhesin. *Proc Natl Acad Sci* **109**: E690–E697.

Zhang, Y., Yuan, Z.-P., Qin, Y., Dai, J., and Zhang, T. (2018) Comparative studies on hydrophilic and hydrophobic segments grafted poly(vinyl chloride). *Chinese J Polym Sci* **36**: 604–611.

Supporting Information

Additional Supporting Information may be found in the online version of this article at the publisher's web-site:

Appendix S1: Supporting Information